METEOROLOGICAL INFORMATION EXTRACTION ALGORITHM FOR SHIP ROUTING

Zhaokun Wei
College of Transportation, Shandong University of Science and Technology, Qingdao, China.

Xinlian Xie
Transportation Management College, Dalian Maritime University, Dalian, China., xxlian77@yahoo.com

Ming Wei
Logistic Management Department, Qingdao Harbour Vocational& Technical College, Qingdao, China

Tiantian Bao
Transportation Management College, Dalian Maritime University, Dalian, China

Follow this and additional works at: https://jmstt.ntou.edu.tw/journal

METEOROLOGICAL INFORMATION EXTRACTION ALGORITHM FOR SHIP ROUTING

Acknowledgements

METEOROLOGICAL INFORMATION EXTRACTION ALGORITHM FOR SHIP ROUTING

Zhaokun Wei[1], Xinlian Xie[2], Ming Wei[3], and Tiantian Bao[2]

ABSTRACT

The meteorological environment plays an important role when optimizing ship routing. Therefore, with the goal of obtaining meteorological environmental data associated with ship routing, an algorithm that can accurately obtain environmental data around a rhumb route in a standardized common data form is proposed. A Mercator projection is a type of equal-angle projection, and a rhumb route is a straight line on a Mercator chart. Consequently, the linear equation for a rhumb route can be achieved using the point-slope form. Based on this linear equation, points with a regular spacing whose degree is determined by the longitudinal size of the grid can be obtained. Then, the points from the Mercator chart are projected to geodetic coordinates. The extracted grids are traversed by the regularly spaced adjacent points with identical degrees of longitude on the rhumb route; therefore, the meteorological environmental data around the rhumb route can be obtained. Finally, the algorithm is executed and verified using MATLAB. The results of the experiments show that the algorithm proposed in this paper can extract wind grid data and effectively address the extraction of other meteorological environmental data. Thus, the algorithm is useful in the selection of ship routes based on a consideration of meteorological factors.

I. INTRODUCTION

Meteorological factors can affect the selection and opti-

mization of ship routes, and the rapid development of the hydrospheric and atmospheric sciences and the enormous increases in the capabilities of computer technology have resulted in many sophisticated operational tools that have improved the accuracy of weather forecasting and climate analyses (Delitala et al., 2010). With the improved resolution and precision of geophysical models, numerical models with higher spatiotemporal resolution have been built. Currently, most meteorological data are published in a common data format, including data from the National Centre for Atmospheric Research and other organizations that are engaged in atmospheric research (Risien and Chelton, 2008).

With access to high-precision meteorological data, many studies have focused on selecting or optimizing ship routes in combination with meteorological factors. In addition, some websites offer commercial services for optimizing ship routes. Optimized ship routing between two points based on wave models and added resistance was proposed by Vlachos and Sen (Vlachos, 2004; Sen and Padhy, 2010). Szlapczynska (Szlapczynska, 2007, 2013; Szlapczynska and Smierzchalski, 2009) obtained optimal weather routing using an isochrones method that selected a route based on multicriteria optimization processes. Wind and wave grid data were used by Kosmas and Panigrahi to optimize ship routes (Kosmas and Vlachos, 2012; Panigrahi et al., 2012). Dynamic programming, which is a well-known path planning method, is also applied to optimize weather routing (Wei et al., 2012; Wei and Zhou, 2012). Both the isochrones method and dynamic programming focus on the meteorological situation between two isochrones or two nodes to optimize the route between two isochrones or two nodes to achieve the optimal route. In other words, the optimization strategies are based on local meteorological information rather than the global meteorological situation around ship routes. Furthermore, with the increasing ease of access to climate data, they have also been used to offer decision-making support and risk evaluation for weather routing.

For example, Yin and Zhang (2006) analysed wind and wave features at the Bohai straits via statistical methods. Campos et al. (2018) proposed extreme wind-wave modelling and analysed the winds and waves of the south Atlantic Ocean. Shi et al. (2019) analysed the wave climate along the Chinese

Table 1. List structure of wind field data

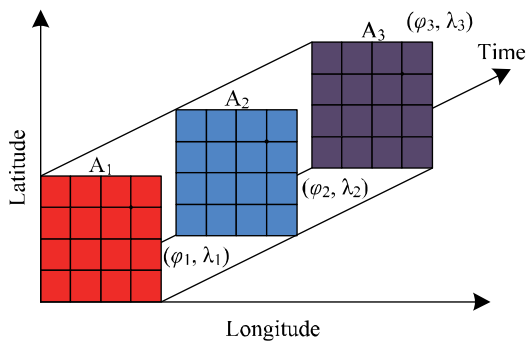| Field Name	Field Description	Type	Bytes	Field Attribute
R	Identified Number	Int	64	Major key
T	Type	Int	64	
LAT	Latitude*600, 000 (°)	Int	64	
LON	Longitude*600,000 (°)	Int	64	
A	Wind Speed*10 (m/s)	Int	64	
B	Meridional Wind Speed*10 (m/s)	Int	64	
C	Zonal Wind Speed*10 (m/s)	Int	64	
D	Wind Direction*600,000 (°)	Int	64	
LTM	Time (YYYYMMDDHHMMSS)	String	14	

Fig 1. Structure of the wind field data in NetCDF

coast with 39-year high-resolution wave data. The global cean wind climate and wave climate were analysed by Young and Donelan (2018), although they mostly focused on global waters or specific water bodies. These studies were not able to acquire ocean climate data around ship routes and could only provide macro data support. As described above, the isochrones method and dynamic programming are mainly utilized to solve the problems involved in optimizing ship routes. However, climate data analysis is used to provide decision-making support and risk evaluations for global or specific waters. It is necessary to propose an algorithm to solve the problems involved in optimizing ship routes, with consideration of the global meteorological situation around specific ship routes, and to provide decision-making support and weather risk evaluations for specific ship routes.

To fill the aforementioned gap, this paper designs a meteorological information extraction algorithm for ship routes. The algorithm is beneficial to extract data from grids with all types of spatial resolutions around ship routes to select the appropriate weather route with consideration of the global meteorological situation to lower fuel consumption and provide decision-making support and weather risk evaluations. To verify the performance of the proposed algorithm, wind data obtained from the University Corporation for Atmospheric Research (UCAR) are used as an example.

II. SHIP ROUTE AND NETCDF

In this section, ship route and Network Common Data Form (NetCDF) characteristics are introduced that form the basis of the proposed algorithm.

1. Ship Route

Two types of ship routes are observed in marine areas: great circle route and rhumb route. A rhumb route is the line between two points on the Earth's surface with a fixed angle between true north and the rhumb route. A great circle route is the shortest path between two points on the Earth's surface, and it is used as the basis of ship routes by ocean going ships. However, because the angles between true north and these great circles are not constant, ship's officers must alter the ship's course frequently to guarantee that ships navigate along the great circle. Therefore, a ship route truly consists of many rhumb routes (Nord and Miller, 1996). Using rhumb routes, ships navigate along each route using a fixed course before altering their course for the next route. Hence, the meteorological data along the great circle route is the same as that along the rhumb routes that constitute the great circle, which means that we can extract meteorological data around a ship route by obtaining the meteorological data along the rhumb route. In other words, the goal of the proposed algorithm is to extract environmental data around rhumb routes.

2. Network Common Data Form

NetCDF is a set of software libraries and self-describing machine-independent data formats that support the creation, access and sharing of array-oriented scientific data. The format itself is an open standard that is commonly used for climatology, meteorology and oceanography applications. The University Corporation for Atmospheric Research is the chief source of NetCDF software, standards development, updates, etc.

A dataset based on NetCDF is typically described via dimensions, variables and attributes, which are then assigned ID numbers. The variables are used to store the data; the dimensions are used to store independent variables; and the attributes are used to store auxiliary information about variables such as units, physical meaning, etc. In essence, a dataset based on NetCDF is a one-value function with a multivariable to store data.

Table 2. Computed instance for a Mercator projection

Starting point	(22.36°N, 122.22°E)	(2.5386e+06, 1.3606e+07)
Endpoint	(28.20°N,125.50°E)	(3.2541e+06, 1.3971e+07)
Straight-line equation	$y - 1.3606e + 07 = 1.96 \times (x - 2.5386e+06)$	
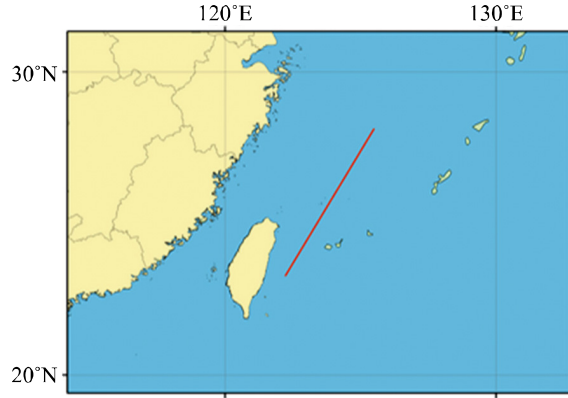
(a) The route presented in Mercator coordinates
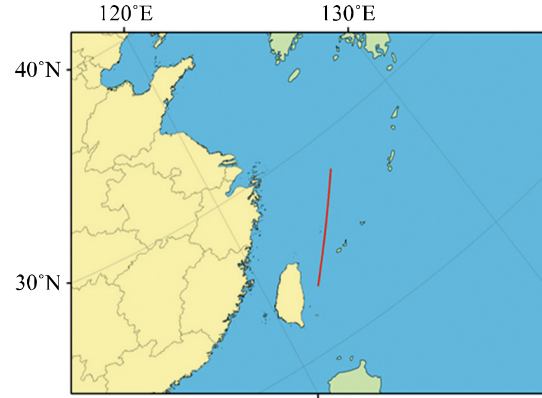
(b) The route presented in WGS87 North Pole LAEA coordinates

Fig 2. Rhumb route in different coordinates

The wind field data used in this paper were obtained from the National Centre for Atmospheric Research (NCAR). These data are stored as NetCDF datasets with a spacing resolution of 0.25° as shown in Fig 1. In Fig 1, latitude, longitude and time are independent variables in NetCDF while wind speed is a variable. We can obtain the wind speed in the grid at the central position at a given time as shown in Eq. (1):

$$wind\_speed = f(time, latitude, longitude) \qquad (1)$$

III. ESTABLISHING A METEOROLOGICAL DATABASE

Different meteorological data may possess different spatial and temporal resolutions. Moreover, these data may also be obtained at different times. To conveniently obtain data with a specific spatial or temporal resolution during a certain period, a database must be built to store meteorological data. Hence, databases are built that have specific list structures. Different meteorological data are equipped with different list structures. To describe the list structures established in the database, the list structure of the wind field data is shown as an example in Table 1.

As shown in Table 1, the central position of every grid is stored in the LAT and LON fields, and different wind speed measurements are stored in the A, B, C, and D fields. The LTM field is used to record local time. The type of meteorological data (e.g., wind, wave or current) is described by T. To guarantee that the data being stored are integers, the position and wind speed are multiplied by different coefficients, which helps reduce memory space requirements.

IV. PROPOSED ALGORITHM

As described in Section 2, a great circle is composed of many rhumb routes and meteorological data are recorded in grids with $n°$ spatial resolution. Hence, we only need to obtain the grids traversed by the rhumb routes that constitute the great circle. In this way, we can obtain the meteorological data around a ship's route.

1. Obtaining a linear equation for a rhumb route

A curve connects two points on the surface of a sphere; however, obtaining the expression that describes the curve when only the starting and ending point of the curve are given is difficult. A rhumb route is a kind of curve that has a fixed angle with the meridian and can be converted into a straight line using the Mercator projection, which is a type of equal-angle projection. This result can be achieved by Eqs. (2)–(6). First, Eqs. (2)–(4) are used to convert the starting and ending point coordinates for the rhumb route into Mercator coordinates (Shi et al., 2009; Xia et al., 2003; Li et al., 2012). Then, the straight-line equation for the rhumb route on the Mercator chart can be expressed in point-slope form as described by Eqs. (5)–(6). Furthermore, the points on the straight line with an $n°$ interval in longitude can be determined using a straight-line equation. According to the relationship between Mercator coordinates and geodetic coordinates, the geodetic coordinates of points on the rhumb route are easy to obtain using the Mercator coordinates of the points on a straight-line, which then allow the determination of which grids a ship route traverses:
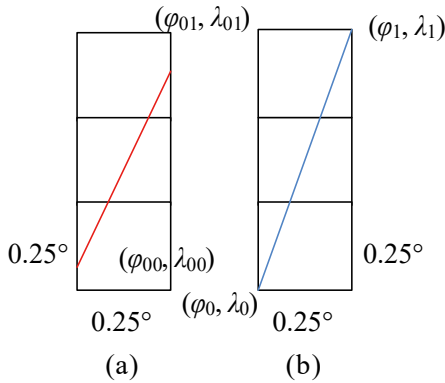
Fig 3. Diagram showing the grids traversed by a rhumb route

$$x = r_0 \lambda \tag{2}$$

$$y = r_0 \ln\left(\tan\left(\frac{\pi}{4} + \frac{\varphi}{2}\right)\left(\frac{1 - e\sin\varphi}{1 + e\sin\varphi}\right)^{e/2}\right) \tag{3}$$

$$r_0 = a / \sqrt{1 - e^2 \sin^2\varphi} \times \cos\varphi \tag{4}$$

where λ denotes longitude, φ denotes latitude, and their units are radians; a is the semimajor axis of an ellipsoid; e is the eccentricity ratio, and x and y are coordinates on a Mercator chart whose units are in meters.

$$\frac{y_m - y_0}{x_m - x_0} = k \tag{5}$$

$$y - y_0 = k(x - x_0) \tag{6}$$

In the above equations, k is the slope, (x_0, y_0) is the starting point, and (x_m, y_m) is the ending point. A computed instance is shown in Table 2, and the rhumb route in Table 2 is presented with different coordinates in Fig 2. In Fig 2(a), the route is presented in Mercator coordinates, and in Fig 2(b), it is presented in WGS84 North Pole LAEA coordinates.

2. Grid extraction

As described in Section 4-1, the substitution of straight-line segments for a rhumb route on a Mercator chart is common practice. To extract the grids through which the rhumb route passes, points on the straight line with an interval of $n°$ in longitude are obtained as shown in Fig 3 and projected onto geodetic coordinates as shown in Eqs. (7)–(9) (Li et al., 2013). Then, based on the two adjacent points in geodetic coordinates, the corresponding grids can be extracted as described below:

$$\lambda = x / r_0 \tag{7}$$

$$\varphi = \varphi' + B_2 \sin 2\varphi' + B_4 \sin 4\varphi' + B_6 \sin 6\varphi' + B_8 \sin 8\varphi' \tag{8}$$

$$\varphi' = 2\arctan\left(e^{\frac{y}{r_0}}\right) - \frac{\pi}{2} \tag{9}$$

where B_2, B_4, B_6 and B_8 are all coefficients.

As shown in Fig 3, the red and blue lines, which have intervals of equal degrees, traverse the same grids, which indicates that the grids traversed by adjacent points with a regular spacing of the same degree in longitude on a rhumb route are related only to the minimum latitude, φ_0, in the grid where the starting point is located and the maximum latitude, φ_1, in the grid where the endpoint is located. Thus, the number of grids traversed can be calculated by Eq. (10).

$$m = \frac{\varphi_1 - \varphi_0}{n} \tag{10}$$

where n is the spacing resolution. In Fig 3, n is 0.25°.

Obtaining the values of (φ_0, λ_0) and (φ_1, λ_1) is the key to extracting the corresponding grids. Both $(\varphi_{00}, \lambda_{00})$ and $(\varphi_{01}, \lambda_{01})$ can be easily obtained because both are on the straight-line that forms the rhumb route. In other words, $(\varphi_{00}, \lambda_{00})$ and $(\varphi_{01}, \lambda_{01})$ are given when the straight line for the rhumb route is determined. Furthermore, the endpoints of the four grids are divisible by the spacing resolution and the decimal parts of the four endpoints are specific numbers. Wind field data provide the best example. The point (-69.875°, 0.125°) is the bottom-left endpoint as the geographical coordinate of a starting wind grid. Because the spacing resolution is 0.25°, the decimal portions of four endpoints of the geographical coordinates are always one of four numbers: 0.125, 0.375, 0.625, and 0.875. Based on the above features, we summarize that (φ_0, λ_0) is the minimum geographic coordinate in the grid that includes $(\varphi_{00}, \lambda_{00})$ with decimal parts (which is within the range [0.125, 0.375), [0.375, 0.625), [0.625, 0.875) or [0.875, 0.125)), and its decimal portion must be 0.125, 0.375, 0.625 or 0.875. Then, it is easy to determine (φ_0, λ_0) because $(\varphi_{00}, \lambda_{00})$ is given. A similar method can be used to obtain (φ_1, λ_1), which is the maximum geographic coordinate in the grid that includes $(\varphi_{01}, \lambda_{01})$. After (φ_0, λ_0) and (φ_1, λ_1) have been determined, the indexes of the data can be calculated as shown in Eqs. (11) – (12). Hence, the indexes of the grids traversed are (i, j), $(i+1, j+1)$ ……$(i+m-1, j+m-1)$. Based on the index values of the grids, the wind field data can then be determined:

$$i = \frac{\varphi - \varphi_b}{n} + 1 \tag{11}$$

$$j = \frac{\lambda - \lambda_b}{n} + 1 \tag{12}$$

where (i, j) is the index and (φ_b, λ_b) is the geographic coordinate of the starting grid data. The index is used to retrieve the wind field data.
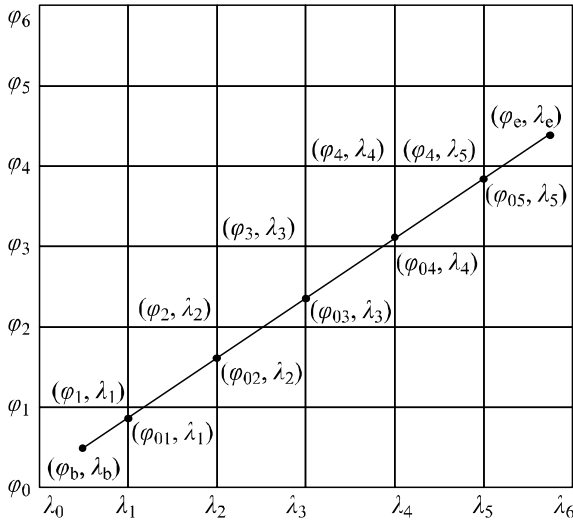
Fig 4. The diagram of a rhumb route

(a) The frequencies of wind scales in Jan, Feb and Mar

(b) The frequencies of wind scales in Apr, May and Jun

(c) The frequencies of wind scales in Jul, Aug and Sep

(d) The frequencies of wind scales in Oct, Nov and Dec

Fig 5. Statistical bar graphs of wind scales

3. Proposed algorithm

The proposed algorithm described in Sections 4-1 and 4-2 can be implemented as follows.

Step 1. Coordinate transformation. The great circle is divided into many rhumb routes using the function gcwaypts in the M_Map toolbox. Then, the endpoints of every rhumb route (e.g., (φ_b, λ_b) and (φ_e, λ_e) in Fig 4) are projected to Mercator coordinates.

Step 2. Obtain the straight-line equation for the rhumb route. Using the endpoints of the rhumb route, the straight-line equation for the rhumb route is determined using the point-slope form as described in Section 4-1.
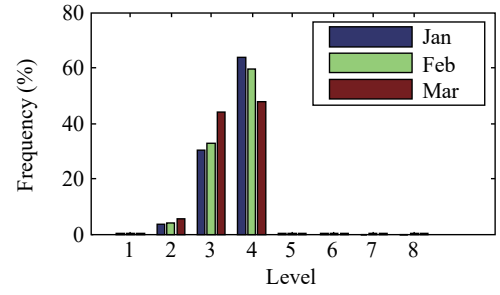
Step 3. Calculate points on the straight lines and project them to geodetic coordinates. Based on the spacing resolution, the points at a certain interval denoted along the straight-line (such as $(\varphi_{01}, \lambda_1)$, $(\varphi_{02}, \lambda_2)$……$(\varphi_{05}, \lambda_5)$ in Fig 4) are projected to geodetic coordinates.

Step 4. Extract the grids and retrieve the wind-field data. As described in section 4-2, the grids traversed by two points with a known interval on the rhumb route can be calculated to obtain the wind grids around the rhumb route. Then, based on the index values of the wind grids, the wind speed or other information can be retrieved.
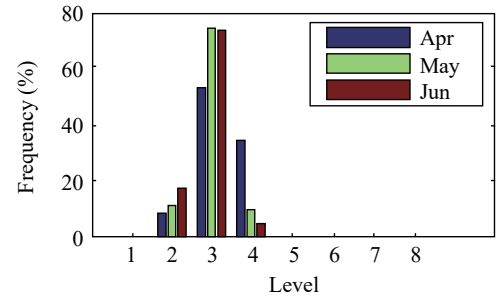
As described above, it is easily concluded that the computational cost of data extraction will increase when the data has a high spatial resolution. Under these circumstances, parallel computing is an efficient measure to lower the computational cost.
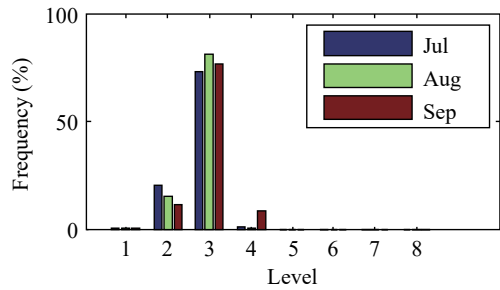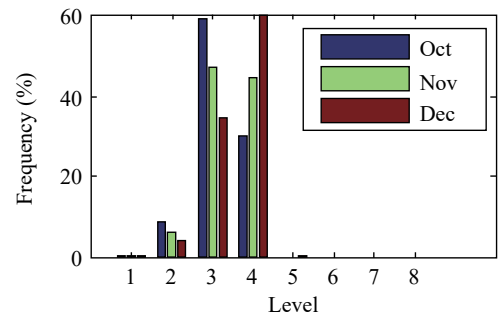
V. EXPERIMENTS

To validate the proposed algorithm, wind field data with 0.25° × 0.25° spatial resolutions from September 1999 to September 2009 were used as an example, and they included the datasets wind_speed_monthly_fields.nc, wind_zonal_monthly_fields.nc and wind_meridional_monthly_field.nc. The records in the first dataset represent the average wind velocity every month over ten years, while the second and third datasets contain the zonal average wind velocity and meridional average wind velocity, respectively. The second and third datasets are used to calculate the wind directions as shown in Eq. (13):

Table 3. Statistical wind field data for the rhumb route

Grids	Wind Speed	Wind Direction	Grids	Wind Speed	Wind Direction
1	9.25 m/s	33.69 °	17	8.94 m/s	38.28 °
2	9.25 m/s	33.69 °	18	8.94 m/s	38.58 °
3	9.20 m/s	33.96 °	19	8.88 m/s	39.09 °
4	9.20 m/s	34.34 °	20	8.88 m/s	39.48 °
5	9.20 m/s	34.69 °	21	8.87 m/s	39.89 °
6	9.17 m/s	34.96 °	22	8.82 m/s	40.42 °
7	9.14 m/s	35.21 °	23	8.79 m/s	40.95 °
8	9.08 m/s	35.51 °	24	8.75 m/s	41.48 °
9	9.05 m/s	35.54 °	25	8.71 m/s	42.27 °
10	9.03 m/s	35.63 °	26	8.67 m/s	43.08 °
11	9.02 m/s	36.08 °	27	8.63 m/s	43.79 °
12	9.01 m/s	36.53 °	28	8.59 m/s	44.55 °
13	8.98 m/s	37.17 °	29	8.57 m/s	45.39 °
14	8.97 m/s	37.52 °	30	8.52 m/s	46.00 °
15	8.95 m/s	38.00 °	31	8.49 m/s	46.75 °
16	8.94 m/s	38.02 °			

$$\begin{cases} \alpha = \text{atan}2(Z_s, M_s) \\ \alpha = \pi / 2 - \alpha \end{cases} \qquad (13)$$

where Z_s is the zonal wind velocity and M_s is the meridional wind velocity. However, α is located in $[-\pi, \pi]$, which is not the true wind direction because its starting point is not the same as the true wind direction. Therefore, it must be converted. In Eq. (13), $\alpha = \pi / 2 - \alpha$ is adopted to change value domain to $[-\frac{\pi}{2}, \frac{3\pi}{2}]$, and then Eq. (14) is used to determine the true wind direction.

$$\begin{aligned} \alpha &= \alpha \times 180/\pi \\ \alpha &= rem(\alpha + 360°, 360°) \end{aligned} \qquad (14)$$

where $rem(\alpha, 360)$ is a function described in Eq. (15):

$$\alpha = \begin{cases} \alpha & \alpha < 360° \\ \alpha - 360° & \alpha \geq 360° \end{cases}. \qquad (15)$$

Based on the dataset, the wind velocity and wind directions are extracted from waters. Its latitude locates from 0°N to 60.25°N and its longitude locates from 120°E to 100°W. The statistical results are illustrated in Figs 5 and 6. Furthermore, wind data and associated statistical results around a rhumb route from (20°N,125°E) to (23°N,130°E) are obtained and used to verify the effectiveness of the proposed algorithm and compare the obtained results with the statistical results from the study area.

In Fig 5, the numbers represent the Beaufort scale. For example, 1 stands for gentle breeze, 2 means a moderate breeze, 3 stands for a fresh breeze, 4 stands for a strong breeze, 5 stands for a moderate gale, 6 stands for a fresh gale, 7 stands for a strong gale, and 8 stands for a whole gale.

In January and February, the area from 0°N~60.25°N and 120°E~100°W is mainly dominated by strong breezes. In March, both fresh and strong breezes prevail. In April, May and June, fresh breezes are frequent. In July, August and September, fresh breezes are also frequent, but in August and September, their frequencies are lower than those in May and June and higher than those in July than in April. These results indicate that the different wind scale frequencies differ across different seasons and that fresh and strong breezes prevail over the entire year.

In Fig 6, 1 stands for [0°, 22.5°); 2 stands for [22.5°, 45°); 3 stands for [45°, 67.5°), etc.

In January, the prevailing wind directions are within the ranges [0°, 22.5°), [22.5°, 45°) and [202.5°, 225°). In February, the prevailing wind directions fall with the ranges [0°, 22.5°) and [22.5°, 45°).

In March, the dominant wind directions lie within the range [0°, 22.5°), [22.5°, 45°) and [180°, 202.5°) but the frequencies of wind directions within the ranges [0°, 22.5°) and [22.5°, 45°) are similar. In April, the prevailing wind directions are within the ranges [0°, 22.5°), [22.5°, 45°) and [180°, 202.5°) and the frequencies of wind directions within the ranges [22.5°, 45°) and [180°, 202.5°) are similar. In May, the prevailing wind directions lie within the ranges [0°, 22.5°), [180°, 202.5°) and [337.5°, 360°). In July, the primary wind directions are within the ranges [0°, 22.5°), [202.5°, 225°) and [337.5°, 360°). In August, the main wind directions are nearly the same and

Table 4. Analysis of the wind field data around a rhumb route

Statistics	Wind Speed	Wind Direction
Mean	8.92 m/s	38.72 °
Std	0.22 m/s	3.89 °

(a) The frequencies of wind directions in Jan, Feb and Mar

(b) The frequencies of wind directions in Apr, May and Jun

(c) The frequencies of wind directions in Jul, Aug and Sep

(d) The frequencies of wind directions in Oct, Nov and Dec
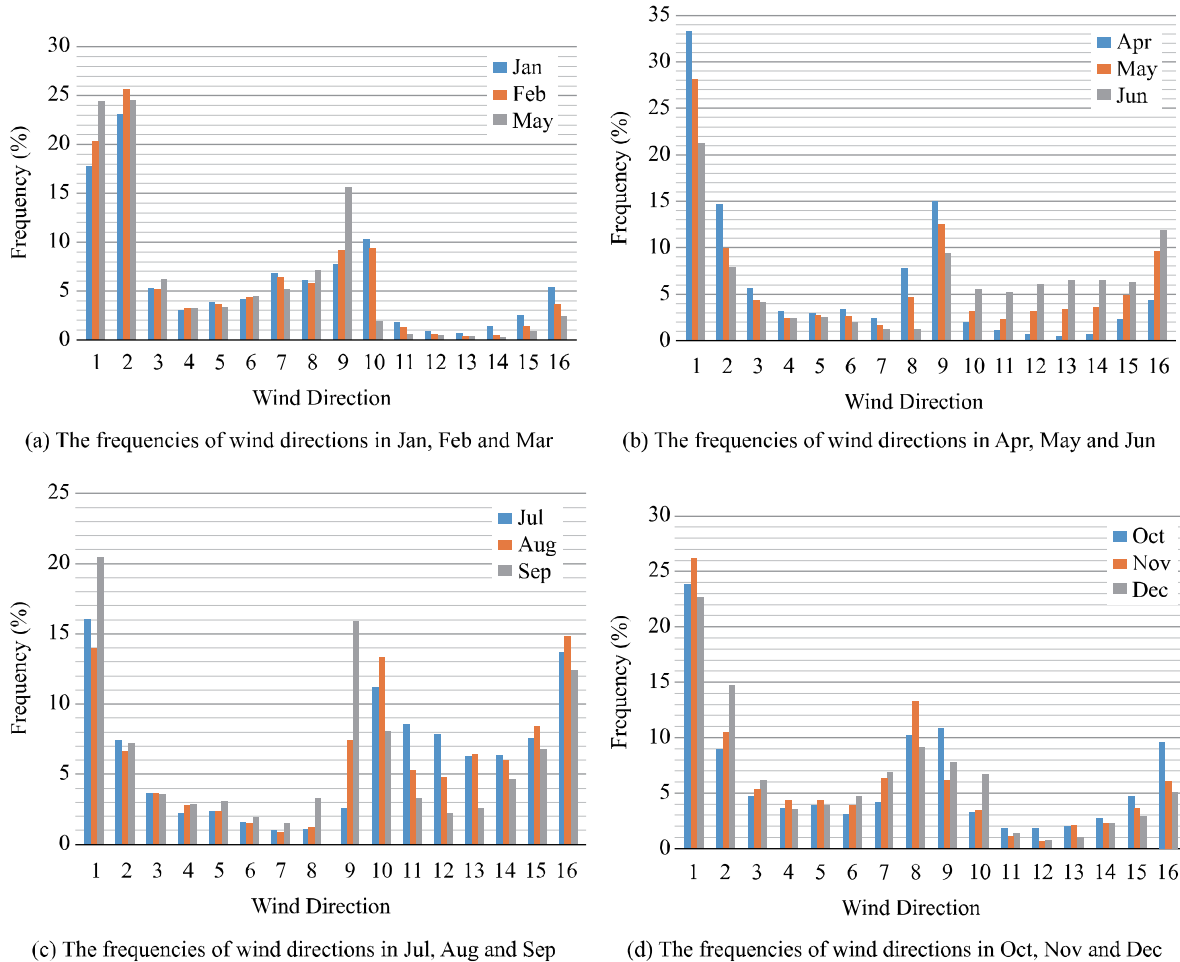
Fig 6. Statistical bar graphs of wind direction

within the ranges [0°, 22.5°), [180°, 202.5°) and [337.5°, 360°). Furthermore, the frequencies of the primary wind directions in August are basically the same. In November and December, the frequencies of wind directions within the ranges [0°, 22.5°), [22.5°, 45°) and [157.5°, 180°) are noticeably higher than that of the other months. In October, the most prevalent wind direction is within the range [0°, 22.5°) and the other four wind directions are roughly the same and within the ranges [22.5°, 45°), [157.5°, 180°), [180°, 202.5°) and [337.5°, 360°). As described above, the main wind directions differ in different months, and there are five main wind directions in terms of the full year.

In Fig 7, the wind data around a rhumb route from (20°N,125°E) to (23°N,130°E) has been extracted, and the grids it passes through are shown with different map scales.

The grids traversed by the rhumb route from (20°N,125°E) to (23°N,130°E) in Fig 7 are shown on an electronic chart with different measuring scales. The measuring scale in Fig 7(a) is 1:4166847, while that in Fig 7(b) is 1:1578518. There are thirty-one grids around the rhumb route. The wind field data for January around the rhumb route are listed in Table 3, and the statistics are listed in Table 4. As indicated in Table 3 and Table 4, fresh breezes surround the rhumb route and the wind directions are within the range [33.69°, 46.75°]. Furthermore, the wind velocity is mostly located within the range of 8.7–9.14 and the wind directions mostly range from 34.83°–42.61°. The maximum wind velocity around the rhumb route is 9.25 m/s, and the minimum wind velocity is 8.49 m/s. Regarding wind directions, the maximum wind direction is 46.75° and the minimum wind direction is 33.69°.
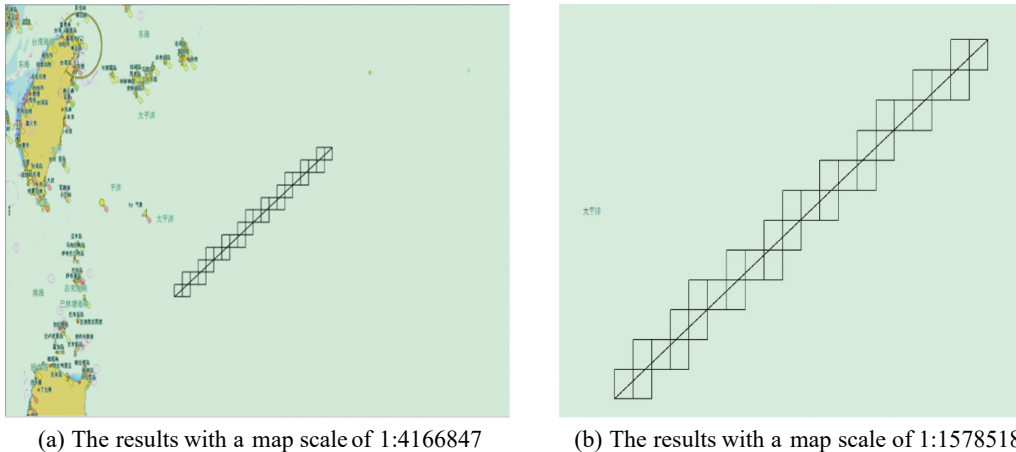
(a) The results with a map scale of 1:4166847   (b) The results with a map scale of 1:1578518

Fig 7. Grids traversed by a rhumb route

The range of 8.7–9.14 m/s falls in the fresh breeze range that prevails in January in the area (0°N,120°E) to (60.25°N, 100°W). The wind direction range of 34.83°–42.61° falls within the range [22.5°, 45°]. A comparison of the results with the wind field data for the area from (0°N,120°E) to (60.25°N,100°W) shows that the scopes of the wind velocity and wind directions around the rhumb route in January are basically same as those in the area from (0°N,120°E) to (60.25°N,100°W). However, the scopes of the former are somewhat smaller than that of the latter. In other words, the wind field data around the rhumb route is more concrete and accurate and thus are useful in selecting or optimizing ship routes. In summary, the proposed algorithm is effective for obtaining meteorological data around ship routes and can obtain meteorological data that are more applicable for selecting or optimizing ship routes.

VI. CONCLUSIONS

On a Mercator projection map, a rhumb route is a straight line, which is the result of equal-angle projection. Based on this concept, this paper proposes an algorithm for obtaining meteorological data around a rhumb route. The proposed algorithm includes three parts. First, to obtain the straight-line equation for the rhumb route, geodetic coordinates are projected onto a Mercator projection map. Second, a straight-line equation for the rhumb route is achieved based on its point-slope form. Third, the points on the straight line are projected to geodetic coordinates and the coordinates of adjacent points are used to extract grids. Finally, wind field data are used as an example for experiments. The wind field data around a rhumb route from (20°N,125°E) to (23°N,130°E) and the wind field data in the area from (0°N,120°E) to (60.25°N,100°W) are both extracted. The results from analysing the former are compared with that of the latter. The results show that more concrete and accurate meteorological data can be easily be obtained by the proposed algorithm. Moreover, the algorithm can be applied to other grid data with

different spatial resolutions. Therefore, the proposed algorithm is beneficial for analysing meteorological conditions in ship routing selection and optimization problems.

REFERENCES

Campos, R.M., J.H.G.M. Alves, G.Guedes Soares and G.E.Parente (2018). Extreme wind-wave modelling and analysis in the south Atlantic ocean. Ocean Modelling 124, 75-93.

Delitala, A. M. S., S. Gallino, L. Villa, K. Lagouvardos and A. Drago(2010). Weather routing in long-distance Mediterranean routes. Theoretical and Applied Climatology 102, 125–137.

Kosmas, O. T. and D. S. Vlachos (2012). Simulated annealing for optimal ship routing. Computers & Operation Research 39, 576–581.

Li, H. P., S. F. Bian and H. H. Li (2012). Expressions of Commonly Used Conformal Projections and Their Analytical Transformations by Complex Numbers. Journal of Geomatics Science & Technology 2, 109-112.

Li, Z. M, S. F. Bian and H. Y. Kong (2013). Symbolic Iterative Method for Solving Inverse Problems in Ellipsoidal Geodesy. Hydrographic Surveying & Charting 33, 27-33.

Nord, J. and E. Miller (1996). Mercator's rhumb lines: a multivariable application of arc length. College Mathematics Journal 27, 348-387.

Panigrahi, J. K., C. P. Padhy, D. Sen, J. Swain and O. Larsen (2012). Optimal ship tracking on a navigation route between two ports: a hydrodynamics approach. Journal of Marine Science and Technology 17, 59–67.

Risien, C. M. and D. B. Chelton (2008). A global climatology of surface wind and wind stress fields from eight years of QuikSCAT Scatterometer Data. Journal of Physical Oceanography 38, 2379–2413.

Sen, D. and C.P. Padhy (2010). Development of a ship weather-routing algorithm for specific application in north Indian Ocean region. The International Conference on Marine Technology, Dhaka, Bangladesh, 21-27.

Shi, J., J. Zheng, C. Zhang, A. Joly, W. Zhang, P. Xu, T. Sui and T. Chen (2019). A 39-year high resolution wave hindcast for the Chinese coast: Model validation and wave climate analysis. Ocean Engineering 183, 224-235.

Szlapczynska, J. (2007). Multiobjective Approach to Weather Routing. In-

ternational Journal on Marine Navigation and Safety of Sea Transportation 1, 273–278.

Szlapczynska, J. (2013). Multicriteria evolutionary weather routing algorithm in practice. International Journal on Marine Navigation and Safety of Sea Transportation 7, 61–65.

Szlapczynska, J. and R. Smierzchalski (2009). Multicriteria optimization in weather routing. International Journal on Marine Navigation and Safety of Sea Transportation 3, 393–400.

Shi, G. Y., G. Z. Zhu, Y. M. Wang and C. Y. Jia (2009). High accurate lgorithm for forward and inverse solution of rthumb line's problem. Journal of Dalian Maritime University 35, 5-9.

Vlachos, D. S. (2004). Optimal ship routing based on wind and wave forecasts. Applied Numerical Analysis & Computational Mathematics 1, 547–551.

Wei, S., P. Zhou and S. Thong (2012). Development of a novel forward dynamic programming method for weather routing. Journal of Marine Science and Technology 17, 239-251.

Wei, S. and P. Zhou (2012). Development of a 3D dynamic programming method for weather routing. International Journal on Marine Navigation

and Safety of Sea Transportation 6, 79-85.

Xia, Y. X., L. Hu, H. Zhou (2003). Research on arithmetic of coordinates transformation in ECDIS. Journal of Engineering Design 5, 299-302.

Yin, W and Y. Zhang (2006). Statistical analysis of wind and wave features at Bohai straits. The Journal of Dalian Maritime University 32, 84-88.

Young, I. R and M. A. Donelan (2018). On the determination of global ocean wind and wave climate from satellite observation. Remote Sensing of Environment 215, 228-241.